Dyes and Pigments 96 (2013) 211–219

Contents lists available at SciVerse ScienceDirect

Dyes and Pigments

journal homepage: www.elsevier.com/locate/dyepig

Spirobenzofluorene linked anthracene derivatives: Synthesis and application in blue fluorescent host materials

Jeang-A. Seo[a], Chil-Won Lee[b], Myoung-Seon Gong[a,*]

[a] Department of Nanobiomedical Science and WCU Research Center of Nanobiomedical Science, Dankook University, Chungnam 330-714, Republic of Korea
[b] Department of Polymer Science and Engineering, Dankook University, 126, Jukjeon-dong, Suji-gu, Yongin, Gyeonggi 448-701, Republic of Korea

ARTICLE INFO

Article history:
Received 25 June 2012
Received in revised form
5 August 2012
Accepted 12 August 2012
Available online 23 August 2012

Keywords:
Blue OLED
Blue host
Spiro[benzo[c]fluorene-7,9′-fluorene]
Color purity
Anthracene
Spirobenzofluorene

ABSTRACT

Blue light-emitting anthracene-based host materials with a spiro[benzo[c]fluorene-7,9′-fluorene] core, 5-(10-(naphthalen-2-yl)anthracen-9-yl)spiro[benzo[c]fluorene-7,9′-fluorene] (**NA-SBFF**) and 5-(10-(4-(naphthalen-1-yl)phenyl)anthracen-9-yl)spiro[benzo[c]fluorene-7,9′-fluorene] (**NPA-SBFF**), were designed and synthesized *via* two-step Suzuki coupling reactions. Introduction of a spiro group into the structure of the anthracene moieties lead to a reduction in crystallization tendency, and a high glass transition temperature was observed. Typical blue fluorescent organic light emitting diodes with the configuration of ITO/*N,N*′-diphenyl-*N,N*′-bis[4-(phenyl-*m*-tolyl-amino)phenyl]biphenyl-4,4′-diamine (DNTPD)/*N,N*′-di(1-naphthyl)-*N,N*′-diphenylbenzidine (NPB)/HOST: Dopant/tris(8-hydroxyquinoline)aluminum (Alq$_3$)/LiF were developed using **SBFF**-type anthracene derivatives as a host material and *N,N,N*′,*N*′-tetraphenylspiro[benzo[c]fluorene-7,9′-fluorene]-5,9-diamine (**TPA-SBFF**) as a dopant material. A device obtained from **NA-SBFF** doped with **TPA-SBFF** showed blue color purity of 0.146 and 0.167, a luminance efficiency of 8.65 cd/A, and an external quantum efficiency >6.01% at 8.0 V.

1. Introduction

Many blue light-emitting dyes have been studied to achieve blue light emissions with host and dopant materials as the emitter, but there is still a clear need for further improvements in terms of stability, efficiency, and color purity [1–3]. Organic electroluminescence (EL) devices using anthracene derivatives as host blue emitters exhibit very promising performance. However, because of the considerable blue shift absorption of these deep blue dopants, better matching host materials with sufficient spectral overlap for efficient Förster energy transfer are needed to facilitate the generation of blue dopant emissions with high efficiency as well as a deep blue color [4,5].

The anthracene plays an important role in the development and application of OLEDs materials such as emitting materials from blue to red, hole- and electron-transporting materials. Recently, their derivatives were reviewed and discussed in relation to the thermal stability and the electroluminescent performance [6–9]. An anthracene based 2-methyl-9,10-di(2-naphthyl)anthracene (MADN) with a stable thin film morphology and a sufficiently wide band gap has been reported. Nevertheless, the color purity is far from adequate for full-color organic light emitting diode (OLED) display applications.

9,10-Di(2-naphthyl)anthracene (β-ADN) is one of the best blue host materials with an efficiency as high as 5.1 cd/A [10]. β-ADN shows excellent stability, the electroluminescent spectrum of the undoped device is broad and featureless and is greenish blue in color centering at 460 nm.

Spiro-type host and dopant materials containing fluorene and benzofluorene as OLED fluorescent materials have received a great deal of attention, because they preserve the inherent characteristics of spiro compound such as morphological stability, high glass transition temperature, and amorphous properties [11–20]. They can also provide a variety of substituents on the spiro[benzo[c]fluorene-7,9′-fluorene] **(SBFF)** because of their asymmetrical spiro core structure with naphthalene, phenyl rings of spiro molecules, and conjugation controlled OLED host materials, as shown in Scheme 1 [21–24].

Many studies have considered **SBFF** as an organic electroluminescent host material. The performance of OLEDs (the color purity and luminescence efficiency) based on **SBFF** is determined by the position of substitution and a variety of aryl moieties with a variety of conjugation chain lengths [25–30].

In this study, a novel anthracene derivative with an **SBFF** core structure was developed as a high fluorescent deep blue host material with good thermal/morphological stability, and the physical properties were investigated. Two new blue host materials consisting of 5-(10-(naphthalen-2-yl)anthracen-9-yl)spiro[benzo

---

* Corresponding author. Tel.: +82 41 5501476; fax: +82 41 5503431.
E-mail address: msgong@dankook.ac.kr (M.-S. Gong).

0143-7208/$ – see front matter © 2012 Elsevier Ltd. All rights reserved.
http://dx.doi.org/10.1016/j.dyepig.2012.08.011

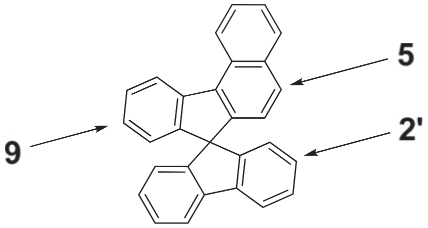

Scheme 1. Substituent positions on spiro[benzo[c]fluorene-7,9′-fluorene].

[c]fluorene-7,9′-fluorene] (**NA-SBFF**) and 5-(10-(4-(naphthalen-1-yl)phenyl)anthracen-9-yl)spiro[benzo[c]fluorene-7,9′-fluorene] (**NPA-SBFF**) were prepared and characterized using ^{1}H nuclear magnetic resonance (NMR), ^{13}C NMR, Fourier transform-infrared (FT-IR), mass spectroscopy (MS), thermal analysis, UV–vis, and photoluminescence (PL) spectroscopy. The EL properties of multi-layered OLEDs fabricated using two host materials and *N,N,N′,N′*-tetraphenylspiro[benzo[c]fluorene-7,9′-fluorene]-5,9-diamine (**TPA-SBFF**) as the dopant were evaluated.

2. Experimental

2.1. Materials and measurements

Tetrakis(triphenylphosphine)palladium(0), (Aldrich Chem. Co., St. Louis, MO, USA), 9,10-dibromoanthracene (TCI Chem. Co., Tokyo, Japan), 4-(naphthalene-1-yl)phenylboronic acid, and naphthalene-2-boronic acid (Frontier Scientific Co., West Logan, UT, USA) were used as received. *n*-Butyllithium (2.5 M solution in hexane), bromine, trimethyl borate (redistilled), potassium carbonate, sodium hydroxide (Duksan Chem. Co., Seoul, South Korea) were used without further purification. 5-Bromospiro[benzo[c]fluorene-7,9′-fluorene] and **TPA-SBFF** were prepared using a method previously reported [01]. Tetrahydrofuran (THF) was purified by distillation over sodium metal and calcium hydride. PL spectra were recorded on a fluorescence spectrophotometer (Jasco FP-6500; Tokyo, Japan) and the UV–vis spectra were obtained by means of a UV–vis spectrophotometer (Shimadzu, UV-1601PC; Tokyo, Japan). Energy levels were measured with a low-energy photo-electron spectrometer (AC-2; Riken-Keiki, Union City, CA, USA). The FT-IR spectra were obtained with a Thermo Fisher Nicolet 850 spectrophotometer (Waltham, MA, USA), and the elemental analyses were performed using a CE Instrument EA1110 (Hindley Green, Wigan, UK). The differential scanning calorimeter (DSC) measurements were performed on a Shimadzu DSC-60 DSC under nitrogen at a heating rate of 10 °C/min. The thermogravimetric analysis (TGA) measurements were performed on a Shimadzu TGA-50 thermogravimetric analyzer at a heating rate of 5 °C/min. The low and high resolution mass spectra were recorded using a JEOL JMS-AX505WA spectrometer in the fast atom bombardment mode. High resolution mass spectra were recorded using an HP 6890 and Agilent 5975C MSD in FAB mode.

2.2. Preparation of 9-bromo-10-(4-(naphthalene-1-yl)phenyl)anthracene

9,10-Dibromoanthracene (10 g, 0.03 mol), tetrakis(triphenyl phosphine)palladium(0) (1.72 g, 1.49 mmol) and 4-(naphthalene-1-yl) phenylboronic acid (7.4 g, 0.03 mol) were dissolved in THF (350 mL) in a double-necked flask and stirred for 30 min. Then, potassium carbonate (2 M, 200 mL) was added dropwise over 20 min. The mixture was degassed and refluxed overnight at 80 °C under a nitrogen atmosphere. After being cooled, the solvent was evaporated under vacuum, and the product was extracted with ethyl acetate and water. The ethyl acetate solution was washed with water and dried with $MgSO_4$. Evaporation of the solvent, followed by column chromatography using *n*-hexane on a silica gel, yielded a white yellow product. 9-Bromo-10-(naphthalene-2-yl)anthracene was prepared using naphthalene-1-boronic acid similar to the procedures described above.

2.3. Preparation of 10-(4-(naphthalene-1-yl)phenyl)anthracene-9-ylboronic acid

9-Bromo-10-(4-(naphthalene-1-yl)phenyl)anthracene (10 g, 21.0 mmol) in dry THF (350 mL) was placed in a double-necked round-bottomed flask (1000 mL) under an argon gas environment. After the reaction mixture was maintained at −78 °C, *n*-BuLi (2.5 M in *n*-hexane, 11.32 mL) was added through a syringe pump over 90 min with vigorous stirring. Trimethyl borate (3.21 mL, 28.0 mmol) in THF (5 mL) was injected through the syringe pump for 30 min. The reaction mixture was raised to room temperature with stirring. After the reaction was completed, 2 N HCl (350 mL) was introduced and maintained for 5 h. The reaction mixture was extracted with ethyl acetate/H_2O (1:1). The organic layer was separated and evaporated to yield a light yellow crystal. 10-(Naphthalene-2-yl)anthracene-9-ylboronic acid was prepared using 9-bromo-10-(naphthalene-2-yl)anthracene using similar procedures to those described above.

2.4. Representative preparation of NPA-SBFF

A solution of 5-bromospiro[benzo[c]fluorene-7,9′-fluorene] (4.51 g, 10 mmol), tetrakis(triphenylphosphine)palladium(0) (0.59 g, 0.51 mmol), and 10-(4-(naphthalene-1-yl)phenyl)anthracene-9-ylboronic acid (4.29 g, 0.01 mol) dissolved in THF (150 mL) was stirred in a double-necked flask for 30 min. Potassium carbonate (2 M, 150 mL) was added dropwise over 20 min. The resulting reaction mixture was refluxed overnight at 80 °C and then extracted with ethyl acetate and water. After the organic layer was evaporated with a rotary evaporator, the resulting powdery product was purified by column chromatography from dichloromethane/*n*-hexane (1/1) to give the yellow **NPA-SBFF** crystalline product. **NA-SBFF** was prepared using similar procedures described above.

2.5. OLED fabrication

A basic device configuration of indium tin oxide (150 nm)/*N,N′*-diphenyl-*N,N′*-bis-[4-(phenyl-m-tolyl-amino)-phenyl]-biphenyl-4,4′-diamine (DNTPD, 60 nm)/*N,N′*-di(1-naphthyl)-*N,N′*-diphenylbenzidine (α-NPB, 30 nm)/host: **TPA-SBFF** (30 nm, *x*%)/2,9-dimethyl-4,7-diphenyl-1,10-phenanthroline (BCP, 5 nm)/Tris(8-hydroxyquinoline)aluminum (Alq_3, 20 nm)/LiF (1 nm)/Al (200 nm) was used for device fabrication, as shown in Fig. 1. The organic layers were deposited sequentially onto the substrate at a rate of 1.0 Å/s by thermal evaporation from heated alumina crucibles. The doping concentration of the dopant materials was varied at 5, 10 and 15%. The devices were encapsulated with a glass lid and a CaO getter after cathode deposition. Current density–voltage luminance and EL characteristics of the blue fluorescent OLEDs were measured with a Keithley 2400 source measurement unit (Cleveland, OH, USA) and a CS 1000 spectroradiometer.

3. Results and discussion

3.1. Synthesis and characterization

TPA-SBFF was prepared as a dopant material using an amination reaction of 5,9-dibromo-**SBFF** and diphenyl amine. 5-Bromo-**SBFF**

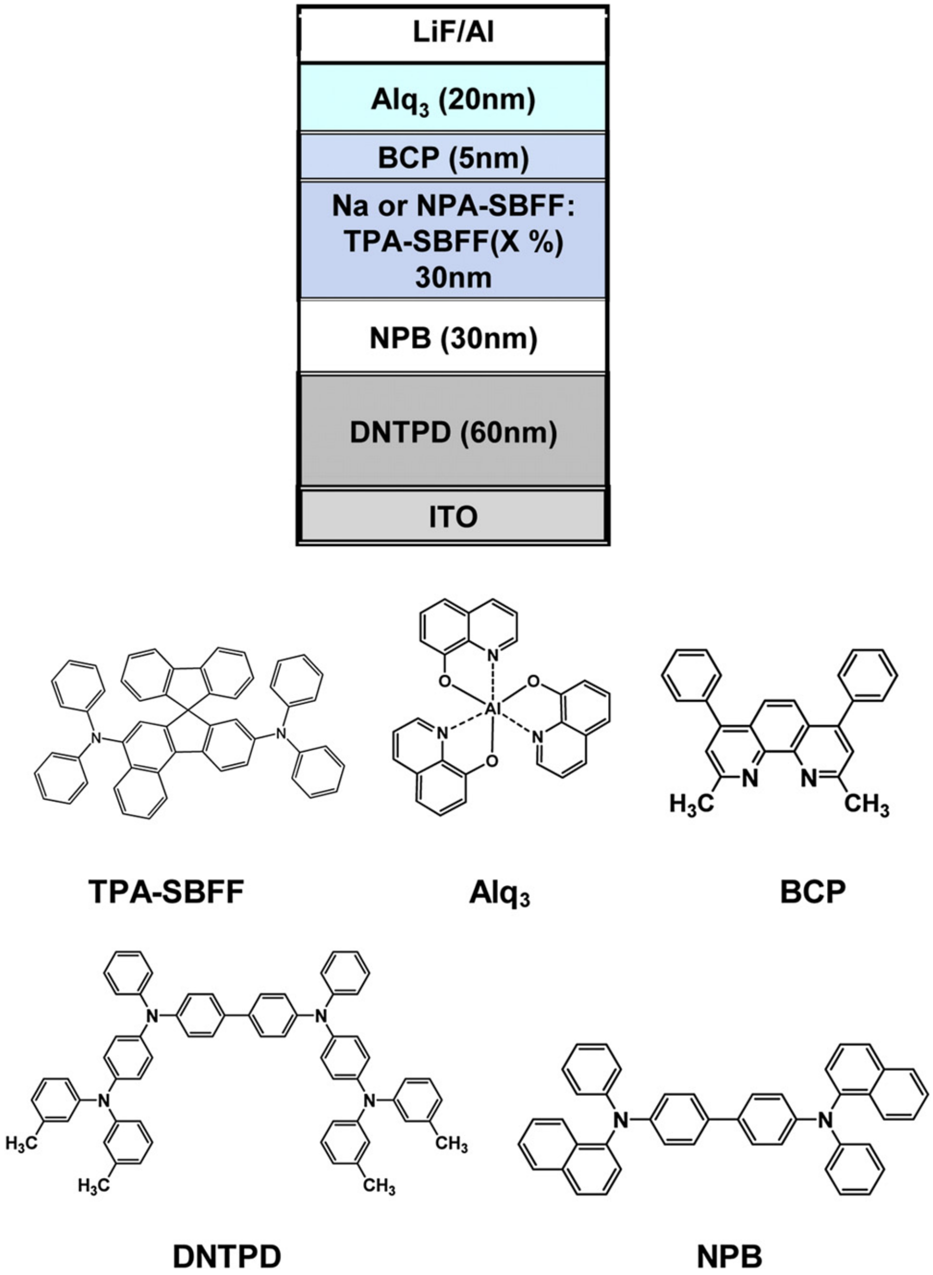

Fig. 1. The device configuration and the chemical structure of the materials used in the devices.

was prepared by selective bromination of **SBFF** in carbon tetrachloride solvent, as shown in Scheme 2. The molecular structures of the anthracene end-capped **SBFF** derivatives and their synthetic routes are shown in Scheme 3. These compounds can be obtained with high yields using typical two-step Suzuki coupling reactions according to a procedure reported previously [21,30]. The chemical structures and composition of the resulting precursors and spiro-compounds were characterized by ^{1}H NMR, ^{13}C NMR, FT-IR, gas chromatography–MS, and elemental analysis.

3.2. Thermal properties

The thermal properties of the resulting blue host materials were characterized by DSC and TGA in a nitrogen atmosphere. The onset decomposition temperatures were 452.0 °C and 433.4 °C for **NA-SBFF** and **NPA-SBFF**, respectively. Table 1 summarizes the DSC and TGA data for the two host materials. The **NPA-SBFF** showed melting points (T_m) of 413 °C, but no melting points were observed on the second heating scan, even though they were given enough time to cool in air. Once the compounds became amorphous solids, they did not revert to the crystalline state. After the samples had cooled to room temperature, a second DSC scan was performed at 10 °C/min and revealed high glass transition temperatures (T_g) of 263 °C and 272 °C for **NA-SBFF** and **NPA-SBFF**, respectively, because of their rigid spiro-type backbone. This result suggests that their thermal stability improved significantly by introducing the rigid anthracene unit into the spiro backbone. As a result, the amorphous glassy state of the transparent films of the two host materials showed that they are good candidates for use as EL materials.

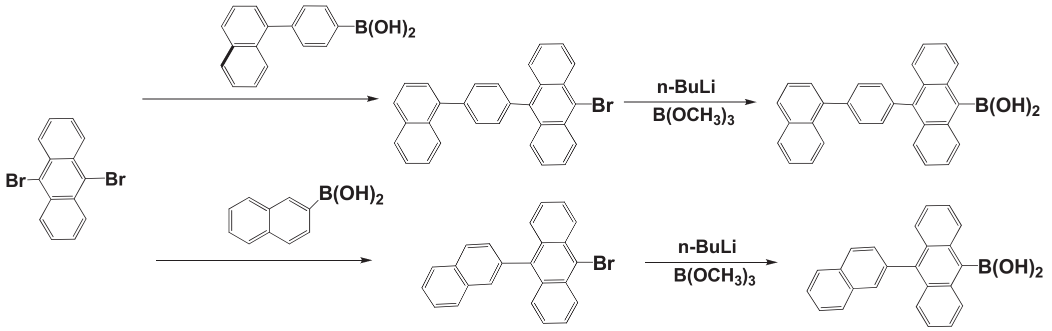

Scheme 2. Preparation of precursors for spiro-type host materials.

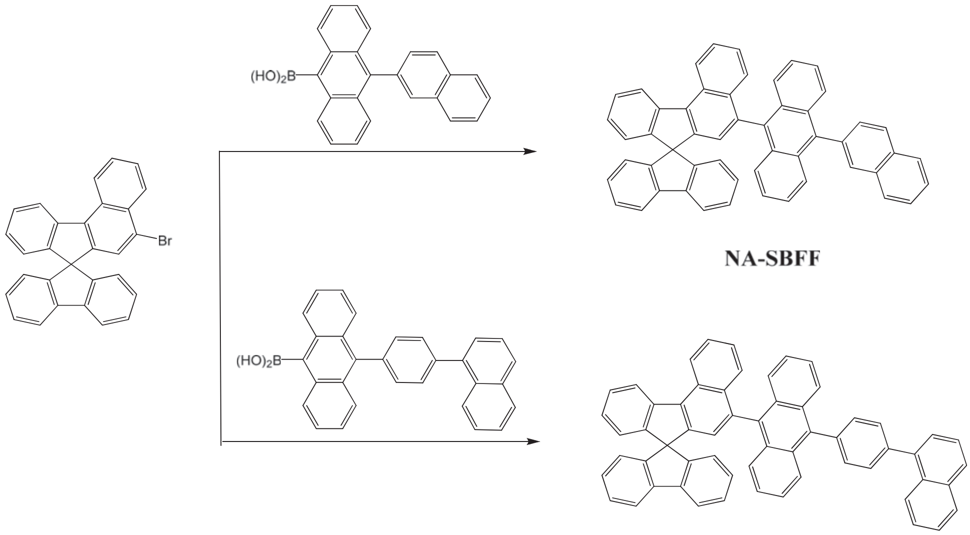

NA-SBFF

NPA-SBFF

Scheme 3. Preparation of **NA-SBFF** and **NPA-SBFF** host materials with **SBFF** and anthracene core.

3.3. *Optical properties and energy levels*

Fig. 2 shows the absorption and fluorescence spectra of the two host materials in dilute THF solution. All absorption spectra had three major bands with similar absorption peaks of 350–400 nm. These characteristic absorption patterns were attributed to the $\pi-\pi^*$ transitions of the central anthracene core of the compounds. The absorption bands at 300–400 nm originated from the combination of the $\pi-\pi^*$ transition of the **SBFF** core and the $\pi-\pi^*$ transitions of the anthracene core. Two compounds exhibited blue emission in solution with a maximum peak of about 435 nm. PL spectra of these compounds in films showed slight red shifts with long tail emission relative to those in solution. For NA-SBFF, there is a clear emission peak at about 650 nm. It seems that the **SBFF** moiety does not minimized intermolecular π-stacking in their solid states. The two hosts produced moderate fluorescence quantum efficiency of 0.72 and 0.59 in dilute cyclohexane solution using 9,10-diphenylanthracene ($\Phi_f = 0.9$ as the reference) from **NA-SBFF** and **NPA-SBFF**, respectively. The photophysical and thermal properties of these compounds are summarized in Table 1. In a previous report, naphthylanthrcenyl group substituted at the 9-position of **SBFF** showed a higher Φ_f value than that of the 5-position. The torsional angle between the phenyl group at the 5-position and that of anthracene was 83.72° [30]. It is well known that a twist angle >90° in **NA-SBFF** and **NPA-SBFF** diminishes or even suppresses the conjugation, which limits fluorescence [31].

A molecular simulation of **NA-SBFF** and **NPA-SBFF** was carried out to understand the physical properties at the molecular level.

Table 1
UV absorption, PL, energy levels and thermal properties of two hosts.

Properties	Sample		NA-SBFF	NPA-SBFF
Purity[a]	HPLC(%)		99.9	99.8
Thermal analysis	DSC	T_g (°C)	263	272
		T_m (°C)	413	439
		T_d (°C)	433.4	452
Optical analysis	UV	Max (nm)	377	376
		Bg[b] (eV)	2.95	2.96
	PL	Max (nm)	436	435
		FWHM[c] (nm)	52.36	52.34
	Solid PL	Max (nm)	449	437
		FWHM[c] (nm)	54.6	50.59
	QE	Φ_f [d]	0.72	0.59
Electrical analysis	AC-2	HOMO (eV)	5.96	5.89
		LUMO (eV)	3.01	2.93

[a] The purity of the samples were finally determined by high performance liquid chromatography (HPLC) using the above prepared samples after train sublimation.

[b] Bandgap.

[c] Full width at half maximum.

[d] Fluorescence quantum efficiency, relative to 9,10-diphenylanthracene in cyclohexane ($\Phi_f = 0.90$).

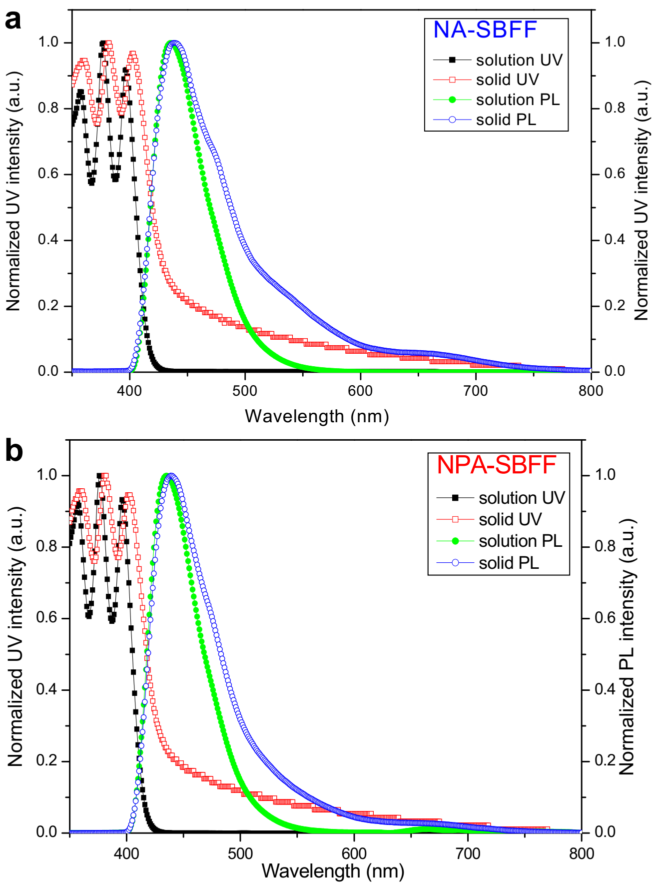

Fig. 2. UV–vis and PL spectra of (a) **NA-SBFF** and (b) **PNA-SBFF**.

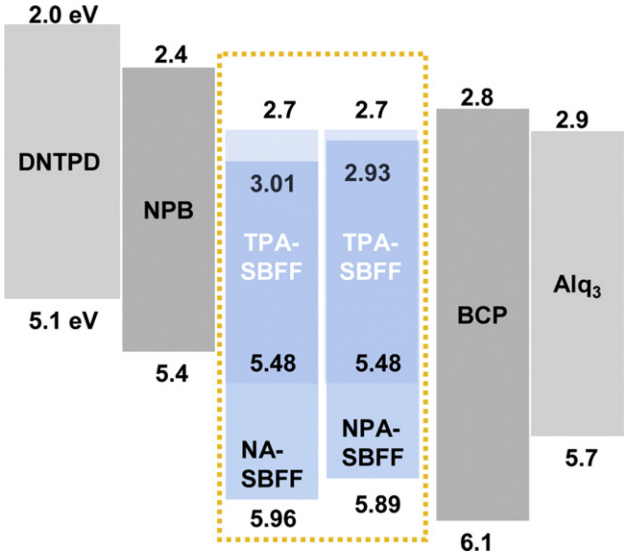

Fig. 4. Energy diagram of the blue fluorescence devices using **NA-SBFF** and **NPA-SBFF**.

Fig. 3 shows the geometric structure of **NA-SBFF** and **NPA-SBFF**. The anthracene core structure was affected by **SBFF** in both **NA-SBFF** and **NPA-SBFF**. Rotation of the spirobifluorene in **NPA-SBFF** and **NA-SBFF** was limited by steric hindrance of the spirobifluorene with anthracene. This lead to distortion of the anthracene core structure, and conjugation of the anthracene core can be destroyed by the spirobifluorene group in **NA-SBFF** and **NPA-SBFF** [32]. Molecular simulation also showed the electron distribution of **NA-SBFF** and **NPA-SBFF**. The highest occupied molecular orbital (HOMO) and the lowest unoccupied molecular orbital (LUMO) distribution of **NA-SBFF** and **NPA-SBFF** are shown in Fig. 3. HOMO and LUMO orbitals of the two host materials were concentrated in the anthracene core, and the substitution position of the spirobifluorene did not affect the HOMO and LUMO distribution in the host materials.

The energy levels of the two host and dopant materials used to fabricate the OLEDs in the present study are shown in Fig. 4. A low-energy photoelectron spectrometer was used to obtain information on the HOMO energies of the host and dopant materials and to examine the charge injection barriers. Energy gaps for **NA-SBFF**, **NPA-SBFF**, and **TPA-SBFF** were calculated as 2.95, 2.96, and 2.71 eV, respectively. The HOMO energy levels

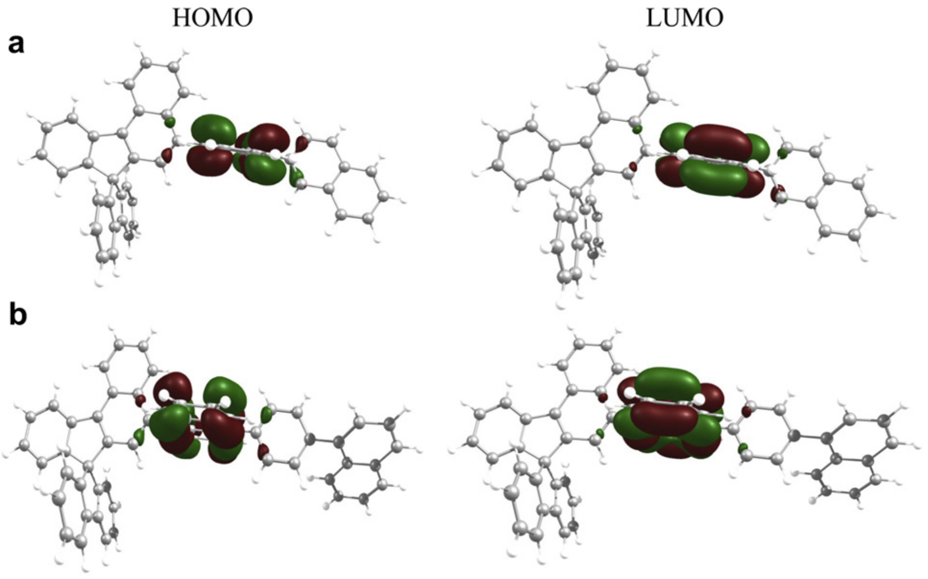

Fig. 3. HOMO and LUMO electronic density distributions of (a) **NA-SBFF** and (b) **NPA-SBFF**, calculated at the DFT/B3LYP/6-31G* for optimization and Time Dependent DFT (TDDFT) using Gaussian 03.

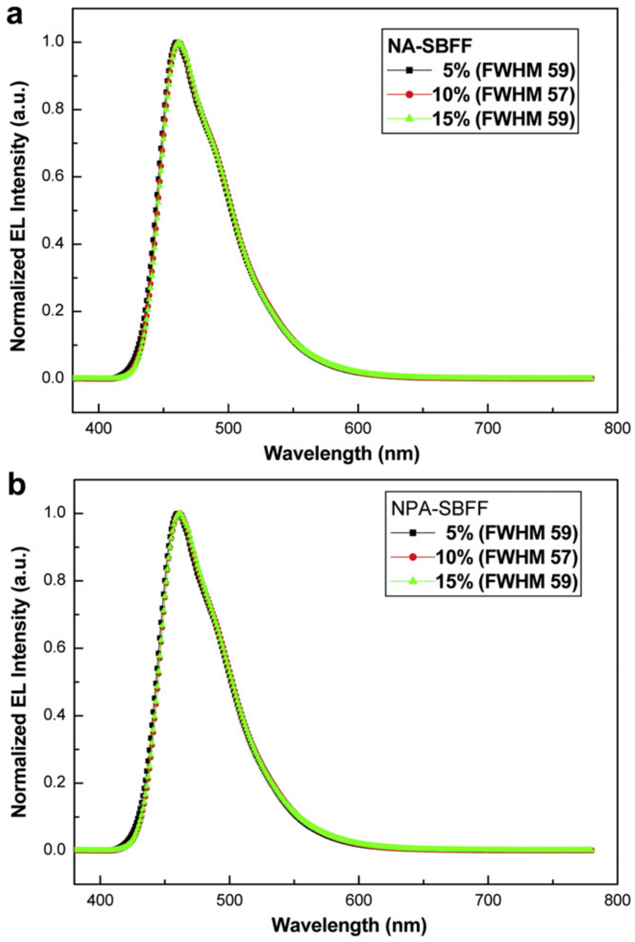

Fig. 5. Electroluminescence spectra of **NA-SBFF** and **NPA-SBFF** devices according to the doping concentration of **TPA-SBFF**.

were −5.89, −5.96, and −5.48 eV for **NA-SBFF**, **NPA-SBFF**, and **TPA-SBFF**, respectively. The HOMO value of **TPA-SBFF** was quite high compared with those of the other two hosts. The HOMO values of the two hosts were similar to those of other anthracene derivatives (−5.5 to −6.0 eV) such as MADN and β-ADN [33].

Table 2
Eelectroluminescence properties of the devices obtained from two host and **TPA-SBF** dopant materials.

Properties	Host	NA-SBFF		NPA-SBFF	
	Dopant	TPA-SBFF			
	(%)	5%	10%	5%	10%
EL at 7 V	λ_{max} (nm)	460	462	460	462
	FWHM (nm)	58.23	57.62	58.14	57.70
	mA/cm^2	0.66	1.37	1.99	3.95
	cd/A[a]	7.92	8.36	7.50	7.15
	cd/A[b]	8.65(8 V)	8.36	7.50	7.47(6 V)
	lm/W[a]	3.55	3.75	3.58	3.18
	lm/W[b]	3.55	3.79(6 V)	3.86(5 V)	3.90(6 V)
	cd/m^2	51.98	114.6	149.7	280.4
	CIE-*x*	0.146	0.145	0.146	0.146
	CIE-*y*	0.167	0.172	0.162	0.169
	EQE(%)[a]	5.47	5.69	5.28	4.88
	EQE(%)[b]	6.01(8 V)	5.69	5.28	5.11(6 V)

[a] Values at 7 V.
[b] Values at a highest peak.

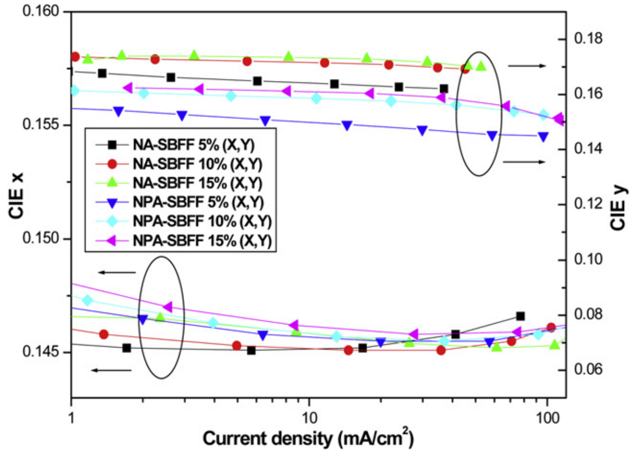

Fig. 6. Stability of the chromaticity depicted by CIE coordination.

3.4. EL properties

The EL spectra of **NA-SBFF** and **NPA-SBFF** doped by the **TPA-SBFF** dopant at different concentrations (5%, 10%, and 15%) were investigated to find the optimum dopant concentration. The EL spectra of the blue fluorescent **NPA-SBFF** device doped with **TPA-SBFF** are shown in Fig. 5, which showed a maximum peak at 460 nm. A blue emission was observed from the **TPA-SBFF**-doped **NPA-SBFF** device, and the color coordinates of the blue device were about 0.146 and 0.167. The EL spectra of other host **NA-SBFF** were quite similar to those of **NPA-SBFF**, as summarized in Table 2. The peak maximum of EL spectra was about 460 nm, and the spectra were consistent even at a high doping concentration. The EL emission was dominated by the emission peak of the dopant. This seemed to indicate that the energy transfer from the host to **TPA-SBFF** dopant was quite efficient at the optimum dopant concentration employed in this experiment. The full width at half maximum of 60 nm was relatively small, which lead to good color purity, as illustrated in the PL spectrum (46–52 nm).

The dependence of chromaticity on current density was measured to evaluate the stability of the devices, as shown in Fig. 6. When the EL spectrum was converted to chromaticity coordinates on the CIE 1931 diagram, chromaticity stability increased with a decrease in dopant concentration. The stability of the CIE*x*

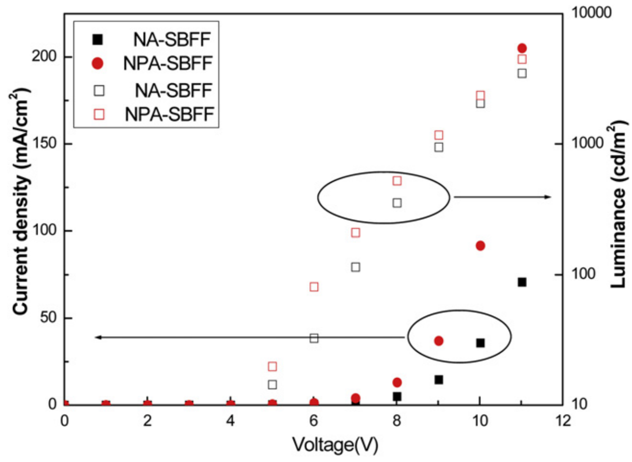

Fig. 7. Current density–voltage–luminescence characteristics of the device using **NA-SBFF** and **NPA-SBFF** doped with 5% **TPA-SBFF**.

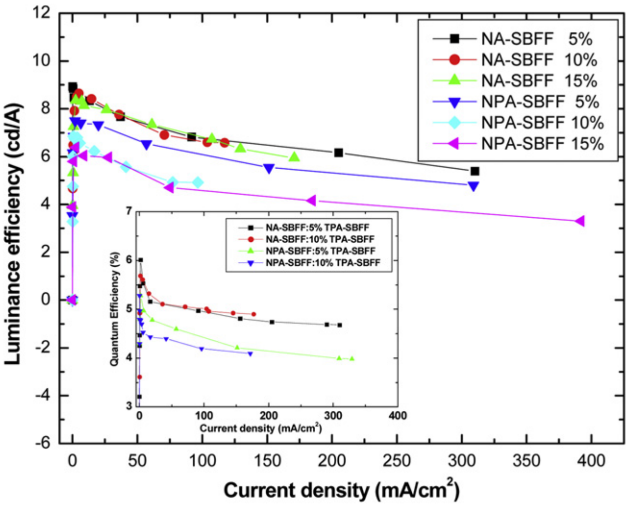

Fig. 8. Current efficiency-current density characteristics of the device using **NA-SBFF** and **NPA-SBFF** doped with 5, 10 and 15% **TPA-SBFF**; the inset is a figure of external quantum efficiency vs current density.

coordinates was better than that of the CIE*y* coordinates. The **NA-SBFF**-based device emitted a blue light with CIE coordinates of 0.146 and 0.167.

3.5. *OLED device properties*

NA-SBFF and **NPA-SBFF** were evaluated as host materials for blue fluorescent OLEDs. **TPA-SBFF** was doped as a blue dopant in the **NA-SBFF** and **NPA-SBFF** host materials, and the device performance of the blue OLEDs was studied. Fig. 7 shows the luminance–voltage–current density characteristics of the OLEDs with two hosts doped with 5% **TPA-SBFF** dopant as the EML. Although the two host materials had similar bandgaps, **NPA-SBFF** showed a slightly higher current density and luminance than that of **NA-SBFF** at the same driving voltage.

As can be seen in the luminance efficiency curves of the six devices in Fig. 8, high efficiencies >6 cd/A were obtained. A low efficiency was observed only in the devices doped with 15% dopant. In the case of the **NA-SBFF** device doped with 10% **TPA-SBFF**, the maximum brightness of 51.98 cd/m^2 and 8.65 cd/A occurred at 8 V, as summarized in Table 2. The maximum quantum efficiency and luminance efficiency of the **NA-SBFF** and **NPA-SBFF** devices were similar. The quantum efficiency >4% maintained at high current density up to 400 mA/cm^2 in the two devices as shown in inset of Fig. 8.

The maximum quantum efficiency of the device obtained from the **NA-SBFF** device doped with 10% **TPA-SBFF** was an external quantum efficiency (EQE) of 5.69%, as shown in Fig. 9. The device showed a maximum power efficiency of 3.75 lm/W, and efficiency increased rapidly to a maximum of approximately 8.36 cd/A at a low current density of 1.37 mA/cm^2 at 7 V. The holes injected from a hole transfer layer, α-NPB, were transferred to the lighting emitting layer and were trapped at dopant sites. The same spiro-type dopant **TPA-SBFF** had a large capacity to catch the holes, and minimized the loss of holes resulting in good EL efficiency. Thus, the HOMO level of **TPA-SBFF** was suitable for hole trapping and hole transporting as a dopant, and the **NA-SBFF** host was moderate for balancing holes and electrons in the emitting layer.

NPA-SBFF doped with 5% **TPA-SBFF** showed high efficiency and a small decrease in efficiency as the current density was increased from 0 to 1.99 mA/cm^2, *i.e.*, a weak-current-induced fluorescent quenching. It reached a current efficiency of 7.50 cd/A, EQE of 5.28%, power efficiency of 3.58 lm/W, and CIE coordinates of 0.146 and 0.162 at 7 V. These results suggest that an exciton was formed and light was emitted at specific thresholds. It should be noted that the efficiencies of these devices remained stable when the luminance was increased to 149.7 cd/m^2.

The PL spectrum of **NA-SBFF** and **NPA-SBFF** overlapped with a major portion of the absorption spectrum of **TPA-SBFF**, as shown

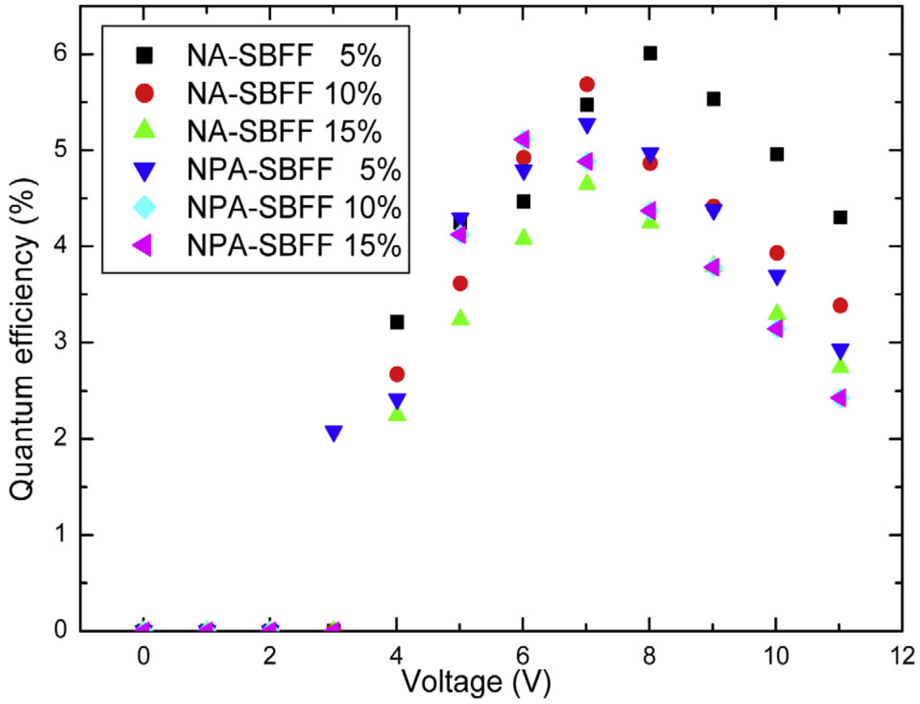

Fig. 9. External quantum efficiency–voltage curves of the **NA-SBFF** and **NPA-SBFF** devices according to the doping concentration of **TPA-SBFF**.

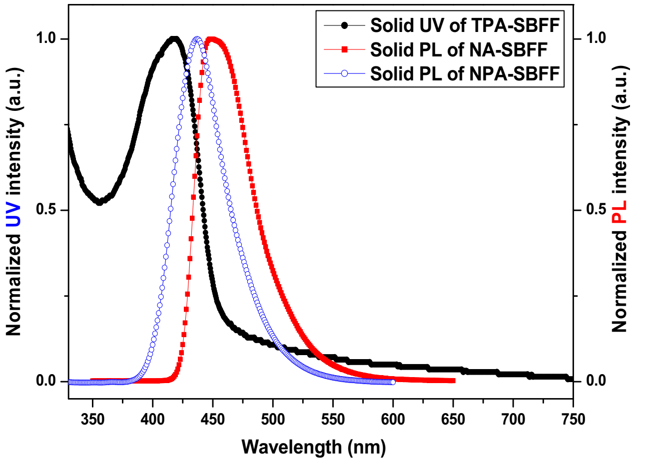

Fig. 10. Overlapping of UV–vis absorption spectrum of **TPA-SBFF** and PL spectra of **NA-SBFF** and **NPA-SBFF**.

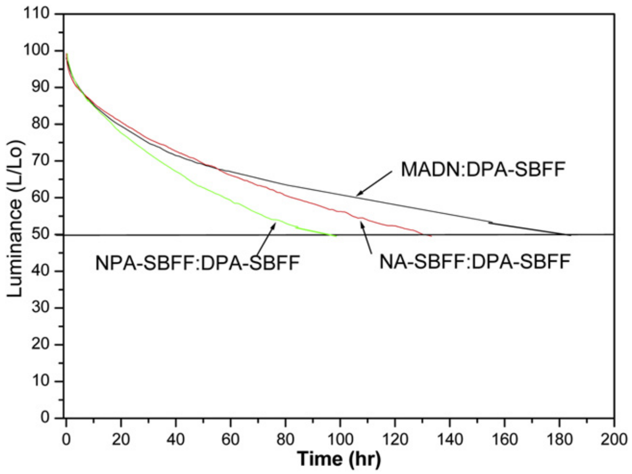

Fig. 11. Lifetime of blue-light emitting devices **MADN**, **NA-SBFF** and **NPA-SBFF** doped with 5% DPA-SBFF.

in Fig. 10. This indicates that **TPA-SBFF** can effectively accept energy from the host through Förster energy transfer or function as a direct recombination center due to the higher HOMO levels. This is one of the highest reported EQE values in blue OLEDs. Combined good efficiency and color purity enabled the dopant materials to be good candidates as blue emitters for OLEDs.

The lifetime of anthracene-liked **SBFF** derivatives was measured as the operational lifetime ($t_{1/2}$) of the blue devices under initial luminance of 3000 cd/m^2 at a constant current. Its lifetime (98 h and 130 h) was less than that of **MADN**: 5% **DPA-SBFF** (180 h) as shown in Fig. 11. Although the vacuum deposited two host films were investigated, the use of the spirobifluorene side group is not advantageous for the morphological stability of the host material. When thermal annealing of the evaporated film was carried out at 150 °C for 15 min, the lifetime was increased up to 160 h. It can be explained by the more stable morphology of the **SBFF** series host materials.

4. Conclusion

New fluorescence blue host materials based on **SBFF** derivatives were successfully prepared and used to construct blue OLEDs. Substitution of the anthracene core on the 5-position of **SBFF** distorted the conjugated structure of the anthracene core and improved glass transition temperatures (T_g) for good thermal stability. The EL emission spectra of the devices was about 462 nm. The typical OLED devices showed excellent performance; the **NA-SBFF**-based device exhibited highly efficient blue-light emission with a maximum efficiency of 8.65 cd/A (EQE, 6.01%). According to these characteristics, these blue light emitting materials have sufficient potential for fluorescent OLED applications.

Acknowledgments

This research was supported by WCU (World Class University) program through the National Research Foundation of Korea funded by the Ministry of Education, Science and Technology (R31-10069).

References

[1] Gao ZQ, Mi BX, Chen CH, Cheah KW, Cheng YK, Wen WS. High-efficiency deep blue host for organic light-emitting devices. Applied Physics Letter 2007;90: 123506–8.

[2] Lee MT, Chen HH, Lian CH, Tsai CH, Chen CH. Stable styrylamine-doped blue organic electroluminescent device based on 2-methyl-9,10-di(2-naphthyl) anthracene. Applied Physics Letter 2007;85:3301–3.

[3] Tao S, Hong Z, Peng Z, Ju W, Zhang X, Wang P, et al. Anthracene derivative for a non-doped blue-emitting organic electroluminescence device with both excellent color purity and high efficiency. Chemical Physics Letters 2004;397: 1–4.

[4] Friend RH, Gymer RW, Holmes AB, Burroughes JH, Marks RN, Salaneck WR. Electroluminescence in conjugated polymers. Nature 1999;397:121–8.

[5] Ho MH, Wu YS, Wen SW, Lee MT, Chen TM, Chen CH, et al. Highly efficient deep blue organic electroluminescent device based on 1-methyl-9,10-di(1-naphthyl)anthracene. Applied Physics Letter 2006;89:252903–5.

[6] Huang J, Su JH, Tian H. The development of anthracene derivatives for organic light-emitting diodes. Journal of Materials Chemistry 2012;22:10977–89.

[7] Xia ZY, Zhang ZY, Su JH, Zhang Q, Fung KM, Lam MK, et al. Robust and highly efficient blue light-emitting hosts based on indene-substituted anthracene. Journal of Materials Chemistry 2010;20:3768–74.

[8] Huang J, Su JH, Li X, Lam MK, Fung KM, Fan HH, et al. Bipolar anthracene derivatives containing hole- and electron-transporting moieties for highly efficient blue electroluminescence devices. Journal of Materials Chemistry 2011;21:2957–64.

[9] Xia ZY, Su JH, Wong WY, Wang L, Cheah KW, Tian H, et al. High performance organic light-emitting diodes based on tetra(methoxy)-containing anthracene derivatives as a hole transport and electron-blocking layer†. Journal of Materials Chemistry 2011;21:8382–8.

[10] Shi J, Tang CW. Anthracene derivatives for stable blue-emitting organic electroluminescence devices. Applied Physics Letter 2002;80:3201–3.

[11] Salbeck J, Yu N, Bauer J, Weissörtel F, Bestgen H. Low molecular organic glasses for blue electroluminescence. Synthetic Metals 1997;91:209–15.

[12] O'Brien DF, Burrows PE, Forrest SR, Konne BE, Loy DE, Thompson ME. Hole transporting materials with high glass transition temperatures for use in organic light-emitting devices. Advanced Materials 1998;10:1108–12.

[13] Salbeck J, Bauer J, Weissörtel F. Spiro linked compounds for use as active materials in organic light emitting diodes. Macromolecular Symposia 1997; 125:121–32.

[14] Katsuma K, Shirota Y. A novel class of π-electron dendrimers for thermally and morphologically stable amorphous molecular materials. Advanced Materials 1998;10:23–6.

[15] Bach U, Cloedt KD, Spreitzer H, Gratzel M. Characterization of hole transport in a new class of spiro-linked oligotriphenylamine compounds. Advanced Materials 2000;12:1060–3.

[16] Ko CW, Tao YT. 9,9-Bis{4-[di-(p-biphenyl)aminophenyl]}fluorene: a high Tg and efficient hole transporting material for electroluminescent devices. Synthetic Metals 2002;126:37–41.

[17] Katsis D, Geng YH, Ou JJ, Culligan SW, Trajkovska A, Chen SH, et al. Spirolinked ter-, penta-, and heptafluorenes as novel amorphous materials for blue light emission. Chemistry of Materials 2002;14:1332–9.

[18] Xiao H, Leng B, Tian H. Hole transport triphenylamine–spirosilabifluorene alternating copolymer: synthesis and optical, electrochemical and electroluminescent properties. Polymer 2005;46:5707–13.

[19] Xiao H, Shen H, Lin Y, Su J, Tian H. Spirosilabifluorene linked bistriphenylamine: synthesis and application in hole transporting and two-photon fluorescent imaging. Dyes and Pigments 2007;73:224–9.

[20] Jiang J, Jiang C, Yang W, Zhen H, Huang F, Cao Y. High-efficiency electrophosphorescent fluorene-alt-carbazole copolymers *N*-grafted with cyclometalated Ir complexes. Macromolecules 2005;38:4072–80.

[21] Kim KS, Jeon YM, Kim JW, Lee CW, Gong MS. Blue light-emitting OLED using new spiro[fluorene-7, 9′-benzofluorene] host and dopant materials. Organic Electronics 2008;9:797–804.

[22] Jeon SO, Jeon YM, Kim JW, Lee CW, Gong MS. Blue organic light-emitting diode with improved color purity using 5-naphthyl-spiro[fluorene-7,9′-benzofluorene]. Organic Electronics 2008;9:522–32.

[23] Kim KS, Jeon YM, Lee HS, Kim JW, Lee CW, Jang JG, et al. Blue organic electroluminescent devices based on the spiro[fluorene-7,90-benzofluorene] derivatives as host and dopant materials. Synthetic Metals 2008;158:870–5.

[24] Jeon YM, Kim JW, Lee CW, Gong MS. Blue organic light-emitting diodes using novel spiro[fluorene-benzofluorene]-type host materials. Dyes and Pigments 2009;83:66–71.

[25] Jeon SO, Jeon YM, Kim JW, Lee CW, Gong MS. Spiro[fluorene-7,90-benzofluorene] host and dopant materials for blue light-emitting electroluminescence device. Synthetic Metals 2009;159:1147–52.

[26] Kim KS, Lee HS, Jeon YM, Kim JW, Lee CW, Gong MS. Blue light-emitting diodes from 2-(10-naphthylanthracene)-spiro[fluorene-7,90-benzofluorene] host material. Dyes and Pigments 2009;81:174–9.

[27] Jeon SO, Yook KS, Joo CW, Son HS, Jang SE, Lee JY. High efficiency red phosphorescent organic light-emitting diodes using a spirobenzofluorene type phosphine oxide as a host material. Organic Electronics 2009;10:998–1000.

[28] Jang SE, Jeon SO, Cho YJ, Yook KS, Lee JY. Stable efficiency roll-off in red phosphorescent organic light-emitting diodes using a spirofluorene–benzofluorene based carbazole type host material. Journal of Luminescence 2010;130:2184–7.

[29] Jeon YM, Lee JY, Kim JW, Lee CW, Gong MS. Deep-blue OLEDs using novel efficient spiro-type dopant materials. Organic Electronics 2010;11:1844–52.

[30] Gong MS, Lee HS, Jeon YM. Highly efficient blue OLED based on 9-anthracenespirobenzofluorene derivatives as host materials. Journal Materials Chemistry 2010;20:10735–46.

[31] Cheon JW, Lee CW, Gong MS, Geum N. Chemiluminescent properties of blue fluorophores containing naphthalene unit. Dyes and Pigments 2004;61:23–30.

[32] Jeon YM, Lee IH, Lee HS, Gong MS. Orange phosphorescent organic light-emitting diodes based on spirobenzofluorene type carbazole derivatives as a host material. Dyes and Pigments 2011;89:29–36.

[33] Wen SW, Lee MT, Chen CH. Recent development of blue fluorescent OLED materials and devices. Journal Display Technology 2005;1:90–9.